TiS Trends in Sciences
TRENDS IN SCIENCES 2027; 24(1): 14254
SPRINT Scholarly Publishing and Repository Integration Center
https://doi.org/10.48048/tis.2027.14254
RESEARCH ARTICLE

Sono-Fenton Delignification of Rice Straw Using Fe_3O_4/GO Nanocatalyst: Process Optimization via Central Composite Design, Reaction Kinetics, and Activation Thermodynamics

Hanif Ardhiansyah[1,2,*], Tutuk Djoko Kusworo[1] and Andri Cahyo Kumoro[1]

[1]Department of Chemical Engineering, Faculty of Engineering, Diponegoro University, Semarang 50239, Indonesia
[2]Department of Chemical Engineering, Faculty of Engineering, Universitas Negeri Semarang, Semarang 50299, Indonesia

([*]Corresponding author's e-mail: hanif.ardhi@mail.unnes.ac.id)

Received: 1 May 2026, Revised: 13 June 2026, Accepted: 23 June 2026, Published: 10 August 2026

Abstract

Rice straw is an abundant lignocellulosic residue whose recalcitrant lignin-silica matrix limits enzymatic conversion to glucose. In this study, a sono-Fenton heterogeneous system employing Fe_3O_4/GO nanocomposite as a magnetically recoverable catalyst was developed for rice straw delignification. A face-centered Central Composite Design with three factors—catalyst dosage (1 - 3 wt%), temperature (40 - 60 °C), and time (20 - 40 min)—was applied to optimize the process. The full quadratic model exhibited excellent predictive performance (R^2 = 0.993, R^2_{adj} = 0.987, R^2_{pred} = 0.956) with non-significant lack of fit. Optimum conditions (2.7 wt%, 58 °C, 37 min) yielded 78.4% delignification with a prediction error of only 1.5%. Temperature was the most influential factor. The synergistic effect of ultrasonic cavitation and Fenton catalysis exceeded the sum of individual treatments by 15.4 percentage points. Delignification kinetics followed pseudo-first-order behaviour with rate constants of 0.015 - 0.031 min^{-1} over 40 - 60 °C. Arrhenius analysis yielded E_a = 31.5 kJ/mol, while Eyring analysis provided $\Delta H^{\ddagger}$ = 28.8 kJ/mol and $\Delta S^{\ddagger}$ = −222 $J \cdot mol^{-1} \cdot K^{-1}$, confirming a chemically controlled, associative mechanism. FTIR spectra confirmed selective lignin removal and partial silica disruption, while SEM revealed pronounced morphological disruption. HPLC analysis of the filtrate showed inhibitor concentrations were below reported inhibitory thresholds. Notably, the process reduced silica by 34.4% while enriching cellulose from 36.5% to 52.8%. These findings establish Fe_3O_4/GO as an effective sono-Fenton catalyst for rice straw delignification, providing integrated kinetic, thermodynamic, and structural evidence for rational process design in lignocellulosic biorefinery applications.

Keywords: Sono-Fenton, Rice straw, Delignification, Fe_3O_4/GO, Central composite design, Reaction kinetics, Activation thermodynamics, Sustainable Development Goals (SDGs)

Introduction

Rice straw (*Oryza sativa*) is one of the most abundant lignocellulosic biomass residues globally, with annual production exceeding 700 million tonnes worldwide and approximately 70 million tonnes in Indonesia alone [1,2]. Despite its significant potential as a renewable feedstock for glucose and bioethanol production, rice straw remains largely underutilized, with open-field burning still practiced in many regions, contributing to air pollution and greenhouse gas emissions [3]. The primary barrier to efficient bioconversion of rice straw lies in its complex lignocellulosic structure, comprising cellulose (35% - 50%), hemicellulose (20% - 30%), lignin (15% - 20%), and a distinctive high silica content (10% - 15%) that collectively create a recalcitrant matrix resistant to enzymatic attack [4,5].

Pretreatment is therefore a critical prerequisite for enzymatic hydrolysis, aiming to disrupt the lignin-

carbohydrate complex, reduce crystallinity, and increase cellulose accessibility [6,7]. Among various pretreatment approaches, ultrasonic-assisted methods have attracted considerable attention due to their ability to generate localized extreme conditions through acoustic cavitation, producing microjet impacts, high shear forces, and reactive radical species—without requiring corrosive chemicals [8]. However, the efficacy of ultrasound alone for lignin removal from high-lignin biomass remains limited, as the mechanical energy from cavitation is often insufficient to cleave the strong ether and carbon–carbon bonds in lignin [9].

To enhance ultrasonic delignification, heterogeneous Fenton catalysis has been integrated with ultrasonication in so-called sono-Fenton systems [10]. In these systems, Fe^{2+}/Fe^{3+} species on the catalyst surface react with H_2O_2 to produce highly reactive hydroxyl radicals (•OH) capable of oxidizing lignin macromolecules [11]. Nanoparticulate Fe_3O_4 (magnetite) is a particularly attractive Fenton catalyst due to its high surface area, redox-active Fe^{2+}/Fe^{3+} sites, and superparamagnetic properties enabling facile magnetic recovery [12]. Nevertheless, bare Fe_3O_4 nanoparticles suffer from aggregation and Fe leaching under ultrasonic conditions, necessitating structural stabilization [13].

Graphene oxide (GO) provides an ideal support for Fe_3O_4 nanoparticles owing to its high surface area, abundant oxygenated functional groups (–COOH, –OH, epoxide), and ability to form Fe–O–C coordination bonds that anchor nanoparticles and prevent aggregation [14,15]. We have previously demonstrated that Fe_3O_4/GO nanocomposites synthesized via co-precipitation exhibit excellent crystallinity, mesoporosity (BET = 152.8 m^2/g), and superparamagnetic behavior (M_s = 60.2 emu/g) with significantly reduced Fe leaching compared to bare Fe_3O_4 [16].

Despite these material advances, comprehensive studies on the application of Fe_3O_4/GO as a sono-Fenton catalyst for rice straw delignification remain scarce. Critical knowledge gaps persist regarding: (i) the systematic optimization of sono-Fenton parameters for rice straw using rigorous statistical design of experiments; (ii) the intrinsic reaction kinetics and activation thermodynamics governing the delignification process; (iii) the fate of hemicellulose and generation of potential inhibitors during pretreatment; and (iv) the effect of sono-Fenton treatment on silica removal—a feature unique to rice straw among common lignocellulosic feedstocks.

The present study addresses these gaps by systematically investigating the sono-Fenton delignification of rice straw using Fe_3O_4/GO nanocatalyst through: (1) process optimization via Central Composite Design (CCD) face-centered with Response Surface Methodology (RSM); (2) pseudo-first-order kinetic modeling at multiple temperatures; (3) Arrhenius and Eyring thermodynamic analysis; (4) quantitative HPLC profiling of hemicellulose-derived products and inhibitors in the pretreatment filtrate; and (5) evaluation of compositional and structural changes in the pretreated biomass through FTIR spectroscopy and SEM imaging, including silica removal. To the best of our knowledge, this study is among the first to integrate kinetic-thermodynamic analysis with silica-removal evaluation for Fe_3O_4/GO-catalyzed sono-Fenton delignification of rice straw.

Materials and methods

Materials

Rice straw (*Oryza sativa* L., IR64 variety) was collected from paddy fields in Semarang, Central Java, Indonesia, after the 2025 dry-season harvest. The straw was washed thoroughly with tap water followed by deionized water, air-dried under shade, milled (Retsch SM 300, Germany) to particle sizes passing through a 40-mesh sieve and retained on a 60-mesh sieve, and oven-dried at 60 °C for 24 h until constant weight. Fe_3O_4/GO nanocomposite (BET = 152.8 m^2/g, crystallite size = 7.6 nm, M_s = 60.2 emu/g) was synthesized via co-precipitation following our previously reported protocol [16]. Iron(III) chloride hexahydrate ($FeCl_3 \cdot 6H_2O$, ≥99%), iron(II) chloride tetrahydrate ($FeCl_2 \cdot 4H_2O$, ≥99%), ammonium hydroxide solution (NH_4OH, 28% (w/w), single-layer graphene oxide (purity >95%), and hydrogen peroxide (H_2O_2, 30% (w/w) were obtained from Sigma-Aldrich (St. Louis, MO, USA) and Merck (Darmstadt, Germany). All other chemicals were of analytical grade and used as received. Deionized water (resistivity >18 MΩ·cm) was used throughout the experiments.

Methods

Sono-Fenton pretreatment

Sono-Fenton pretreatment was performed in a GT-Sonic Ultrasonics, China, 400 W nominal operating at a fixed frequency of 40 kHz. The operating power was set to 200 W. It should be noted that this value represents the nominal electrical input to the transducer; the actual acoustic power delivered to the reaction medium was not calibrated by calorimetric methods in the present study. This limitation is acknowledged in the discussion of the reaction mechanism (see Synergistic effect of ultrasound and catalyst) and in the conclusions.

In each pretreatment run, 5.0 g of dried rice straw (dry basis) was suspended in 100 mL of deionized water (solid-to-liquid ratio of 1:20 w/v) in a 250-mL borosilicate glass reactor. The Fe_3O_4/GO catalyst was added at the designated dosage (1 - 3 wt% of dry straw, see Experimental design and statistical analysis), followed by addition of 1 mL of 30% H_2O_2. The initial pH was adjusted to 5.5 ± 0.1 using 0.1 M HCl, monitored with a calibrated pH meter (Mettler-Toledo FiveEasy F20, Switzerland). The reactor was placed at a fixed position in the centre of the ultrasonic bath, with the liquid level inside the reactor matched to the water level in the bath to ensure consistent acoustic coupling between runs. Reactor temperature was controlled by circulating water through an external jacket connected to a thermostatic bath (Julabo F25, Germany), maintaining the set temperature (40, 50, or 60 ± 0.5 °C) throughout sonication, with continuous monitoring by a Type-K thermocouple inside the reactor. Pretreatment time was varied between 20 and 40 min according to the experimental design (Experimental design and statistical analysis).

After completion, sonication was stopped, and the catalyst was magnetically recovered using a Nd–Fe–B permanent magnet. The remaining solid biomass was separated from the liquid phase by vacuum filtration through Whatman No. 41 filter paper, washed repeatedly with deionized water until the filtrate reached neutral pH (~7.0), and oven-dried at 60 °C for 24 h to constant weight. The recovered solid was used for compositional, spectroscopic, and morphological characterization (Analytical methods), while the combined filtrate from sonication and washing was collected, made up to a known volume, and analysed by HPLC for hemicellulose-derived sugars and inhibitor compounds (HPLC analysis of pretreatment filtrate).

Three sets of control experiments were conducted under otherwise identical optimum conditions to deconvolute the contributions of ultrasound and Fenton catalysis: (i) ultrasound only, in which neither Fe_3O_4/GO catalyst nor H_2O_2 was added, isolating the mechanical-cavitational effect; (ii) Fenton only, in which the same catalyst dosage and H_2O_2 loading were applied without ultrasonic irradiation, with the slurry maintained at the optimum temperature under magnetic stirring (300 rpm); and (iii) the combined sono-Fenton treatment representing the optimum condition. All pretreatment runs were performed in triplicate and results are expressed as mean ± standard deviation.

Experimental design and statistical analysis

A face-centered Central Composite Design (CCD) with $\alpha = 1$ was employed to model the effects of three independent factors on delignification: Catalyst dosage (X_1, 1 - 3 wt% of dry rice straw), pretreatment temperature (X_2, 40 - 60 °C), and pretreatment time (X_3, 20 - 40 min). The design comprised 8 factorial points, 6 axial points, and 6 replicates at the center point, yielding a total of 20 experimental runs. The response variable was the degree of delignification (Y, %), defined as:

$$Y\ (\%) = [(L_0 \times m_0 - L_t \times m_t) / (L_0 \times m_0)] \times 100 \quad (1)$$

where L_0 and L_t are lignin contents (% (w/w), dry basis) before and after pretreatment, and m_0 and m_t are the corresponding solid masses, accounting for solid recovery effects. A second-order polynomial model was fitted:

$$Y = \beta_0 + \Sigma\beta_i X_i + \Sigma\beta_{ii} X_i^2 + \Sigma\beta_{ij} X_i X_j + \varepsilon \quad (2)$$

ANOVA, lack-of-fit testing, model diagnostics, and three-dimensional response surfaces were generated using Design-Expert software version 13 (Stat-Ease Inc., Minneapolis, MN, USA). Numerical optimization was performed using the desirability function approach to maximize delignification within the experimental ranges. Optimum conditions were validated experimentally in triplicate.

Kinetic and thermodynamic analysis

Delignification kinetics were investigated at three temperatures (40, 50, and 60 °C) using the optimum catalyst dosage (2.7 wt%) determined from CCD optimization. For each temperature, separate batch runs were conducted at five sampling times (0, 10, 20, 30, and 40 min). Each sampling time corresponded to an independent experiment terminated at that specific time, rather than aliquot sampling from a single run, in order to avoid disturbance of the reactor's acoustic field and to ensure consistent solid recovery for compositional analysis. Each timepoint was performed in triplicate. Residual lignin content at each sampling time (L_t) was determined gravimetrically using the Van Soest acid-detergent lignin (ADL) method [17]. Pseudo-first-order kinetics were tested by fitting:

$$\ln(L_t/L_0) = -kt \quad (3)$$

where k (min^{-1}) is the apparent first-order rate constant. The temperature dependence of k was analyzed using the linearized Arrhenius equation, $\ln k = \ln A - E_a/(RT)$, and activation thermodynamic parameters were derived from the linearized Eyring equation, $\ln(k/T) = \ln(k_B/h) + \Delta S^{\ddagger}/R - \Delta H^{\ddagger}/(RT)$, where $k_B = 1.381\times10^{-23}$ $J\cdot K^{-1}$ is the Boltzmann constant and $h = 6.626\times10^{-34}$ J·s is Planck's constant. For the Eyring analysis, k was converted from min^{-1} to s^{-1} so as to be dimensionally consistent with the k_B/h prefactor (2.084×10^{10} $s^{-1}\cdot K^{-1}$). The activation Gibbs free energy was calculated as $\Delta G^{\ddagger} = \Delta H^{\ddagger} - T\Delta S^{\ddagger}$.

Analytical methods

Compositional analysis

Cellulose, hemicellulose, and lignin contents were determined by the Van Soest fiber detergent method [17] (NDF–ADF–ADL sequential analysis), in which hemicellulose was calculated as the difference between neutral-detergent fiber (NDF) and acid-detergent fiber (ADF), cellulose as the difference between ADF and acid-detergent lignin (ADL), and lignin as the ADL fraction corrected for residual ash. All compositional determinations were carried out in triplicate and expressed on an oven-dry weight basis. Moisture and total ash were determined according to ASTM E871-82 (oven-drying at 103 - 105 °C to constant mass) and ASTM E1755 (ignition in a muffle furnace at 575 ± 25 °C to constant mass), respectively. Silica content was quantified gravimetrically as the acid-insoluble fraction of the ash: the ash residue was first digested with 10% (w/w) HCl to remove acid-soluble minerals, and the remaining fraction was treated with 50% (w/w) NaOH to selectively dissolve and re-precipitate silica, which was then washed, ignited at 575 ± 25 °C, and weighed to constant mass [18].

Crystallinity index (XRD)

X-ray diffraction patterns were recorded on Shimadzu MAXima_X XRD-7000 using Cu-Kα radiation (λ = 1.5418 Å) at 40 kV and 30 mA, over the 2θ range of 5° - 60° with a step size of 0.02. The crystallinity index (CrI) was calculated using the Segal empirical method [19]: $CrI\ (\%) = [(I_{002} - I_{am})/I_{002}]\times100$, where I_{002} is the maximum intensity at $2\theta \approx 22.5°$ (cellulose I crystalline plane) and I_{am} is the minimum intensity at $2\theta \approx 18°$ (amorphous region).

Fourier-Transform Infrared Spectroscopy (FTIR)

Functional group changes upon pretreatment were assessed by Fourier-transform infrared (FTIR) spectroscopy using Shimadzu IRTracer-100. Samples were prepared as KBr pellets (1:100 sample-to-KBr mass ratio) and spectra were recorded over the wavenumber range of 4,000 - 400 cm^{-1} with a resolution of 4 cm^{-1} and 64 scans co-added per spectrum.

Scanning electron microscopy (SEM)

Surface morphology of raw and pretreated rice straw was examined using a scanning electron microscope at the Physics Laboratory of Universitas Negeri Semarang, operating at 15 kV with a magnification of 3000x and a working distance of 8.9 mm. Prior to imaging, samples were sputter-coated with a thin layer of gold to prevent charging.

HPLC analysis of pretreatment filtrate

Glucose, xylose, arabinose, cellobiose, acetic acid, furfural, and 5-hydroxymethylfurfural (HMF) in the pretreatment filtrate were quantified by high-performance liquid chromatography on a Shimadzu LC-20AD system equipped with an Aminex HPX-87H column (300×7.8 mm, Bio-Rad, USA). The mobile phase was 5 mM H_2SO_4 at a flow rate of 0.6 mL/min, with the column oven maintained at 60 °C. Sugars and

acetic acid were detected with a refractive index detector (RID-10A), while furfural and HMF were monitored simultaneously by a UV-Vis detector (SPD-20A) at 280 nm. Filtrate samples were filtered through a 0.22 μm PVDF membrane prior to injection. Quantification was performed using external calibration curves prepared from analytical standards (Sigma-Aldrich) with linear ranges of 0.1 - 10 g/L ($R^2 > 0.999$) for all analytes.

Results and discussion

Rice straw characterization

The chemical composition of raw rice straw is summarized in **Table 1**. The cellulose content (36.5 ± 1.2%) represents the primary carbon source for glucose production, while the lignin fraction (18.2 ± 0.8%) constitutes the target of delignification. The high silica content (12.5 ± 0.6%)—a distinctive feature of rice straw compared to other lignocellulosic feedstocks—forms a physical barrier on the epidermal surface that impedes catalyst and enzyme penetration [20].

Table 1 Chemical composition of raw rice straw (dry weight basis).

Component	Content (wt%)	Method
Cellulose	36.5 ± 1.2	Van Soest (ADF–ADL)
Hemicellulose	24.8 ± 1.0	Van Soest (NDF–ADF)
Lignin	18.2 ± 0.8	Van Soest (ADL)
Silica (SiO_2)	12.5 ± 0.6	Ashing + selective dissolution
Total ash	16.0 ± 0.5	ASTM E1755
Extractives	4.2 ± 0.3	Sequential extraction
Moisture	8.5 ± 0.4	ASTM E871-82

CCD optimization of sono-Fenton pretreatment

The CCD experimental matrix and delignification results are presented in **Table 2**. Delignification ranged from 32.5% (Run 1: Minimum conditions) to 78.4% (Run 8: Maximum conditions), demonstrating that all three factors significantly influence the process. The six center points (Runs 9, 10, 17-20) yielded consistent values (69.2% - 71.7%, SD = 0.87%), confirming excellent experimental reproducibility.

Table 2 CCD face-centered experimental matrix and delignification results.

Run	X_1 (wt%)	X_2 (°C)	X_3 (min)	Delignification (%)
1	1	40	20	32.5
2	3	40	20	45.2
3	1	60	20	48.6
4	3	60	20	62.1
5	1	40	40	46.8
6	3	40	40	58.2
7	1	60	40	63.5
8	3	60	40	78.4
9*	2	50	30	70.2
10*	2	50	30	69.8
11	3	50	30	74.5
12	1	50	30	57.3
13	2	60	30	75.5

Run	X_1 (wt%)	X_2 (°C)	X_3 (min)	Delignification (%)
14	2	40	30	55.5
15	2	50	40	72.6
16	2	50	20	60.0
17*	2	50	30	71.7
18*	2	50	30	70.7
19*	2	50	30	69.2
20*	2	50	30	70.5

*Center point.

The ANOVA results (**Table 3**) confirmed that the quadratic model is highly significant ($p < 0.0001$) with a non-significant lack of fit ($p = 0.0752$), indicating adequate model representation. The coefficient of determination ($R^2 = 0.993$), adjusted R^2 (0.987), and predicted R^2 (0.956) demonstrated excellent fitting quality and predictive capability. The full quadratic coded Eq. is:

$$Y = 70.73 + 6.97X_1 + 8.99X_2 + 7.11X_3 + 0.54X_1X_2 + 0.01X_1X_3 + 0.49X_2X_3 - 5.39X_1^2 - 5.79X_2^2 - 4.99X_3^2 \quad (4)$$

Table 3 ANOVA for the CCD quadratic model of delignification.

Source	df	SS	F-value	*p*-value	Sig.
Model	9	2763.43	167.96	< 0.0001	***
X_1 (Dosage)	1	485.81	265.75	< 0.0001	***
X_2 (Temperature)	1	808.20	442.11	< 0.0001	***
X_3 (Time)	1	505.52	276.54	< 0.0001	***
X_1X_2	1	2.31	1.26	0.2871	ns
X_1X_3	1	0.0012	0.0007	0.9797	ns
X_2X_3	1	1.90	1.04	0.3319	ns
X_1^2	1	79.92	43.72	< 0.0001	***
X_2^2	1	92.22	50.45	< 0.0001	***
X_3^2	1	68.50	37.47	0.0001	***
Residual	10	18.28	-	-	-
Lack of fit	5	14.67	4.06	0.0752	ns

*** $p < 0.001$; ** $p < 0.01$; * $p < 0.05$; ns = not significant. Non-significant interaction terms (X_1X_2, X_1X_3, X_2X_3) were retained in the full quadratic model. All quadratic terms were significant ($p \leq 0.0001$), confirming pronounced response surface curvature.

Based on coefficient magnitudes, the order of factor influence was: Temperature (8.99) > time (7.11) > catalyst dosage (6.97). The dominance of temperature is attributable to two synergistic mechanisms: (i) enhanced Fenton reaction kinetics at elevated temperatures, accelerating •OH generation from Fe^{2+}/Fe^{3+} cycling with H_2O_2; and (ii) reduced medium viscosity at higher temperatures, intensifying cavitation and improving mass transfer of reactive species to the biomass surface. The negative quadratic coefficient for dosage ($X_1^2 = -5.39$, $p < 0.0001$) indicates an optimum beyond which excess Fe_3O_4/GO acts as a radical scavenger, consuming •OH radicals before they react with lignin—a phenomenon well-documented in heterogeneous Fenton systems [21]. Response surface plots (**Figure 1**) visualize these relationships.

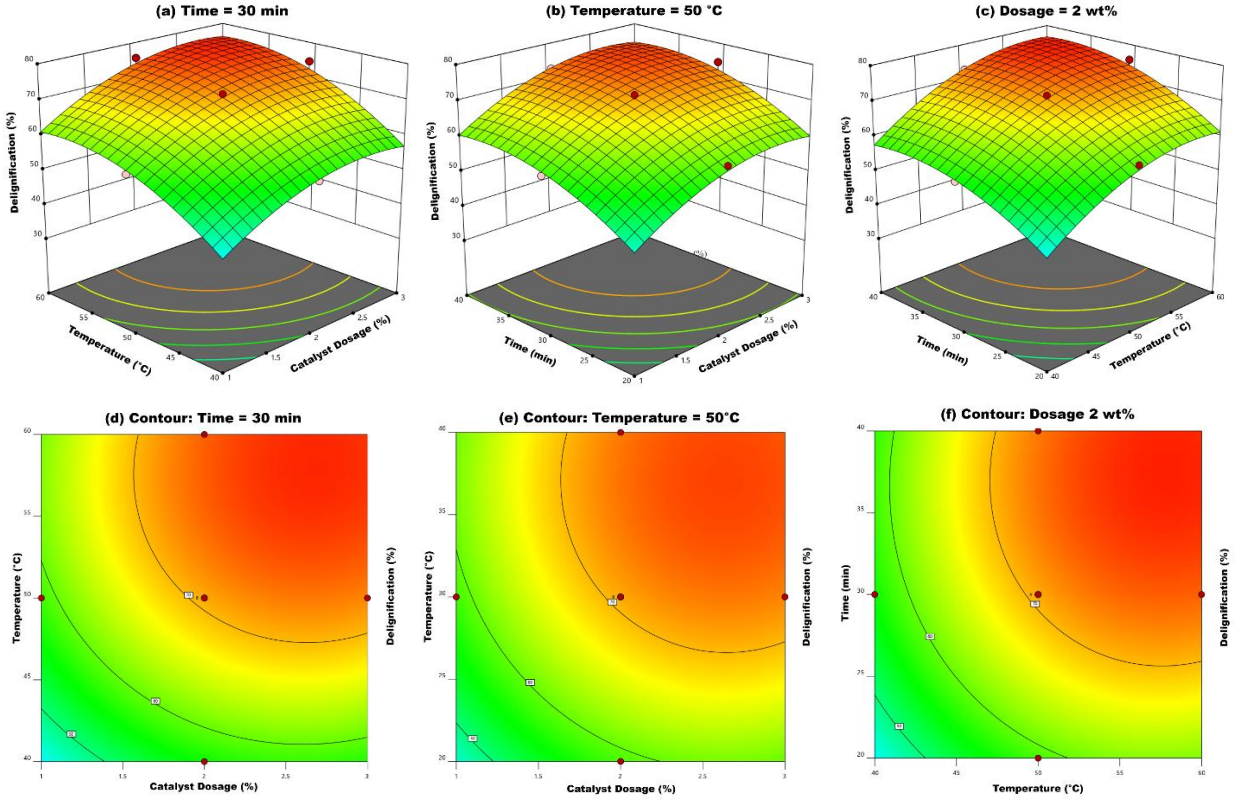


Figure 1 Response surface 3D plots (a - c) and contour plots (d - f) showing the effects of (a,d) dosage-temperature, (b,e) dosage-time, and (c,f) temperature-time on delignification at the center level of the third factor.

Numerical optimization using the desirability function yielded optimum conditions of 2.7 wt% Fe_3O_4/GO, 58 °C, and 37 min, predicting 79.6% delignification. Experimental validation (n = 3) yielded 78.4 ± 1.8%, corresponding to a prediction error of only 1.5%.

Synergistic effect of ultrasound and catalyst

Control experiments were conducted under optimum conditions to quantify the synergistic contribution (**Table 4**). The combined sono-Fenton treatment (78.4%) significantly exceeded the sum of individual treatments (28% + 35% = 63%), yielding a synergy factor of +15.4 percentage points. This synergy can be attributed predominantly to a radical-mediated mechanism, in which ultrasonic irradiation enhances the steady-state concentration of reactive oxygen species (•OH, HO_2•) on the Fe_3O_4/GO surface through three concurrent pathways: (i) supplementing externally added H_2O_2 with additional H_2O_2 generated *in situ* from water sonolysis; (ii) continuous regeneration of catalytically active surface sites through enhanced mass transfer of reactants and removal of adsorbed intermediates; and (iii) prevention of catalyst aggregation, maintaining the dispersed surface area accessible for the Fenton cycle. While bulk acoustic effects such as microjet formation and localized hotspots are characteristic of ultrasonic systems, their contribution at 40 kHz in a bath configuration is expected to be more moderate than at lower frequencies in probe systems, and the chemical (radical) pathway is likely the dominant contributor to the observed synergy [22].

Table 4 Synergistic effect of ultrasound and Fe_3O_4/GO catalyst on delignification.

Condition	Delignification (%)	Interpretation
Ultrasound only (no catalyst)	28.0 ± 1.5	Mechanical cavitation only
Catalyst only (no ultrasound)	35.0 ± 2.0	Conventional Fenton at low T
Ultrasound + Fe_3O_4/GO	78.4 ± 1.8	Sono-Fenton synergy
Synergy factor	**+15.4 pp**	**Exceeds additive effect**

Delignification kinetics and activation thermodynamics

The pseudo-first-order kinetic model (**Figure 2(a)**) provided excellent fits at all three temperatures (R^2 > 0.988), with rate constants increasing from 0.015 to 0.031 min^{-1} over 40 - 60 °C (**Table 5**). The approximate two-fold increase in *k* over a 20 °C range indicates moderate thermal sensitivity, characteristic of catalytic oxidation reactions. The positive temperature dependence is governed primarily by the chemistry of the Fenton cycle rather than by cavitation intensity: Raising the temperature accelerates the regeneration of Fe^{2+} from Fe^{3+} at the catalyst surface and increases the rate of hydroxyl-radical generation and subsequent attack on the lignin macromolecule, consistent with the moderate E_a of 31.5 kJ/mol that is diagnostic of a surface-reaction-controlled regime rather than a diffusion-limited one. Although a higher temperature also lowers the viscosity and surface tension of the medium, conditions that favour bubble nucleation, it simultaneously raises the vapour pressure inside the cavitation bubbles, which cushions their implosive collapse and attenuates the local energy released. Within the 40 - 60 °C range studied, the net enhancement of delignification therefore reflects the dominance of accelerated radical chemistry over any change in cavitation intensity.

The pseudo-first-order treatment is justified by the reaction conditions, in which H_2O_2 and the catalyst-generated hydroxyl radicals were present in large stoichiometric excess relative to the residual lignin; their concentrations are therefore effectively invariant over the reaction window, so the delignification rate reduces to first order in lignin alone. The high linearity of the ln (L_t/L_0) versus time plots (R^2 > 0.988) across the entire temperature range supports this simplification. Accordingly, the pseudo-first-order model was adopted as the simplest expression consistent with the experimental data, and no higher-order formulation was required to describe the delignification profiles within the conditions investigated.

Table 5 Pseudo-first-order rate constants and Arrhenius/Eyring parameters.

T (°C)	T (K)	k (min^{-1})	R^2	ln k	1/T×10^3 (K^{-1})
40	313.15	0.015	0.991	−4.200	3.193
50	323.15	0.022	0.994	−3.817	3.095
60	333.15	0.031	0.988	−3.474	3.002

Derived parameters (Figures 2(b) and 2(c)): E_a = 31.5 kJ/mol and ln A = 7.90 from the Arrhenius plot; $\Delta H^{\ddagger}$ = 28.8 kJ/mol, $\Delta S^{\ddagger}$ = −222 $J \cdot mol^{-1} \cdot K^{-1}$ and $\Delta G^{\ddagger}$ = 98.4 - 102.9 kJ/mol at 313 - 333 K from the Eyring plot, with k expressed in s^{-1}.

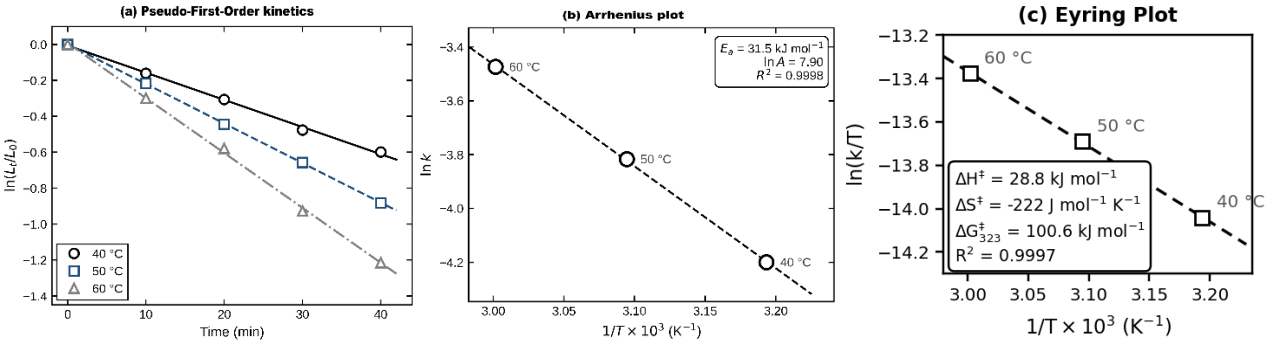


Figure 2 (a) Pseudo-first-order kinetic plots at 40, 50, and 60 °C; (b) Arrhenius plot; (c) Eyring plot for sono-Fenton delignification of rice straw.

The Arrhenius plot (**Figure 2(b)**) yielded E_a = 31.5 kJ/mol, which falls within the range reported for sono-Fenton oxidation of organic substrates (20 - 60 kJ/mol) and is substantially lower than uncatalyzed ultrasonic delignification (50 - 80 kJ/mol) [23]. This reduction confirms the catalytic contribution of Fe_3O_4/GO in lowering the activation barrier via an alternative reaction pathway involving surface-generated •OH radicals.

The Eyring analysis (**Figure 2(c)**) provided activation enthalpy $\Delta H^{\ddagger}$ = 28.8 kJ/mol and activation entropy $\Delta S^{\ddagger}$ = −222 J·mol^{-1}·K^{-1}. The positive $\Delta H^{\ddagger}$ confirms the existence of an appreciable energy barrier to formation of the activated complex, reflecting the energy required to cleave the ether and C–C linkages of lignin; it denotes the activation enthalpy and should not be interpreted as the overall reaction enthalpy. The strongly negative $\Delta S^{\ddagger}$ indicates a highly ordered transition state, consistent with a heterogeneous Fenton mechanism in which reactants (lignin and •OH) must adsorb and orient on the catalyst surface before reaction proceeds—an associative mechanism that reduces molecular degrees of freedom [24]. The Gibbs free energy of activation ($\Delta G^{\ddagger}$ = 98.4 - 102.9 kJ/mol at 313 - 333 K) is dominated by the entropic term, indicating that the spatial orientation of reactants on the catalyst surface—rather than bond-breaking energy—is the rate-limiting factor.

HPLC analysis of pretreatment filtrate

The pretreatment filtrate was analyzed to assess hemicellulose solubilization and inhibitor generation (**Table 6**). The presence of xylose (3.8 g/L) and arabinose (1.2 g/L) confirms partial hydrolysis of the arabinoxylan fraction, consistent with the amorphous nature of hemicellulose being more susceptible to degradation. Critically, inhibitor concentrations remained well below established toxicity thresholds: furfural (0.45 g/L) was below the 1.0 g/L critical level for cellulase inhibition, and HMF (0.12 g/L) was negligible [25]. These values fall well below the inhibitory thresholds commonly reported for enzymatic hydrolysis and microbial fermentation of lignocellulosic hydrolysates (furfural ≈ 1.0 g/L, HMF ≈ 1.0 - 2.0 g/L, acetic acid ≈ 3.5 - 5.0 g/L) [26,27], indicating that the filtrate is compatible with downstream processing without a dedicated detoxification step. Acetic acid (0.9 g/L) from O-acetyl deacetylation was far below the 5.0 g/L threshold. These results indicate that the sono-Fenton pretreatment generates a filtrate that is compatible with downstream enzymatic hydrolysis without detoxification.

Table 6 HPLC analysis of pretreatment filtrate at optimum conditions.

Component	Concentration (g/L)	Source	Inhibition threshold
Xylose	3.8	Hemicellulose hydrolysis	N/A
Arabinose	1.2	Arabinoxylan side-chain	N/A
Acetic acid	0.9	O-acetyl deacetylation	5.0 g/L
Furfural	0.45	Pentose dehydration	1.0 g/L
HMF	0.12	Hexose dehydration	2.0 g/L

Inhibition thresholds are indicative values compiled from the literature on lignocellulosic hydrolysate inhibitors [26,27].

These findings have important implications for analytical methodology. The presence of xylose (3.8 g/L) as a reducing sugar underscores the necessity of HPLC rather than DNS for glucose quantification in subsequent hydrolysis experiments, as DNS-based total reducing sugar measurements would overestimate glucose yield by including hemicellulose-derived sugars [28].

Compositional and crystallinity changes

Table 7 summarizes the compositional and structural changes in rice straw after pretreatment under optimum conditions. Lignin decreased dramatically from 18.2% to 5.1% (a 72% reduction in lignin content, corresponding to 78.4% delignification on a mass basis, Eq. (1)), while hemicellulose decreased from 24.8% to 15.2% (a 39% reduction in hemicellulose content). Cellulose was enriched from 36.5% to 52.8% (+45% relative increase)—a consequence of preferential removal of non-cellulosic components. Notably, silica content decreased by 34.4% on a composition basis (12.5% → 8.2%)—a finding of particular significance for rice straw, since silica deposits on the epidermal surface form physical barriers that restrict catalyst and enzyme access to interior cellulose fibers [20]. The sono-Fenton process partially disrupts this silica layer through combined mechanical shockwaves from cavitation and localized chemical attack at the silica–biomass interface.

Table 7 Composition and structure of rice straw before and after pretreatment under optimum conditions.

Parameter	Before	After	Change (%)	Significance
Cellulose (wt%)	36.5	52.8	+44.7	Enriched for hydrolysis
Hemicellulose (wt%)	24.8	15.2	−38.7	Partially solubilized
Lignin (wt%)	18.2	5.1	−72.0	Primary target achieved
Silica (wt%)	12.5	8.2	−34.4	Unique to rice straw
CrI (%)	42.0	58.0	+38.1	Amorphous phase removed

The increase in crystallinity index (CrI, 42% → 58%) is an apparent effect arising from the preferential removal of amorphous components (hemicellulose, lignin) rather than an increase in intrinsic cellulose crystallinity. While higher CrI is generally associated with reduced enzymatic digestibility, this effect is more than compensated by the dramatic increase in cellulose content, removal of lignin barriers, and disruption of the silica layer—collectively expected to enhance cellulose accessibility for downstream enzymatic hydrolysis. Direct verification of enzymatic digestibility, and particularly the specific contribution of silica removal to hydrolysis yield, was beyond the scope of the present study and is the subject of ongoing work.

FTIR spectroscopic analysis

FTIR spectra of rice straw before and after sono-Fenton pretreatment are presented in **Figure 3**,

providing molecular-level evidence supporting the compositional changes summarized in **Table 7**. The spectra exhibit characteristic absorption bands of lignocellulosic biomass, with several diagnostic peaks showing pronounced changes upon pretreatment, consistent with selective removal of lignin and partial disruption of the silica layer.

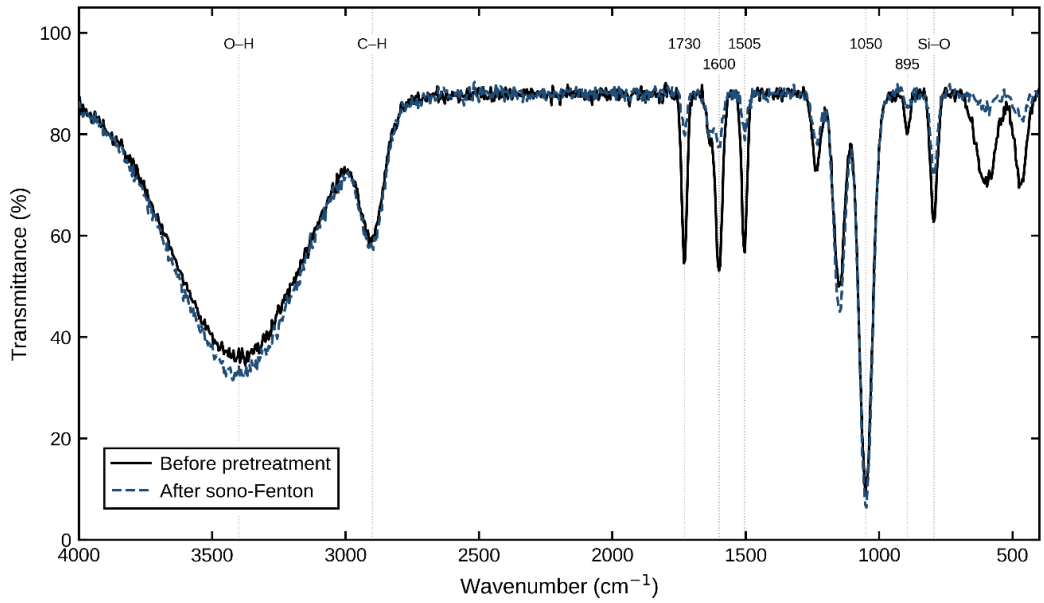


Figure 3 FTIR spectra of rice straw before (blue) and after (red) sono-Fenton pretreatment under optimum conditions, showing reduction of lignin-associated bands at 1,730, 1,600, and 1,505 cm^{-1}, partial reduction of the Si–O band at 795 cm^{-1}, and relative enhancement of the cellulose C–O–C band at 1,050 cm^{-1}.

The most diagnostic changes occur in the lignin-associated region (1,800 - 1,500 cm^{-1}). Three characteristic lignin bands exhibit substantial attenuation following pretreatment: the carbonyl (C=O) stretching band at ~1,730 cm^{-1}, attributable to ester linkages between lignin and hemicellulose as well as carbonyl groups in the lignin side chain; the aromatic ring vibration at ~1,600 cm^{-1} (C=C stretching of the lignin guaiacyl/syringyl units); and the aromatic skeletal vibration at ~1,505 cm^{-1}, which is the most diagnostic single-frequency marker of lignin in lignocellulosic materials [29]. All three lignin-associated bands exhibited a pronounced reduction in band intensity following pretreatment, in qualitative agreement with the 72% reduction in lignin content determined gravimetrically by the ADL method (**Table 7**). Because the spectra were not internally normalised to an invariant reference band, these intensity changes are interpreted qualitatively and are not taken as a quantitative measure of lignin removal.

In the cellulose region, the C–O–C glycosidic linkage band at ~1,050 cm^{-1} became substantially deeper after pretreatment (transmittance dropped from ~10% to ~7%), reflecting the relative enrichment of cellulose in the residual solid following the preferential removal of lignin and amorphous hemicellulose. The β-glycosidic linkage band at ~895 cm^{-1} remained well preserved, confirming that the cellulose backbone integrity was not compromised by the oxidative pretreatment—a critical requirement for downstream enzymatic hydrolysis. The broad O–H stretching band centred at ~3,400 cm^{-1} remained prominent in both spectra, with a slight intensification after pretreatment that is consistent with increased exposure of cellulose hydroxyl groups previously masked within the lignin–carbohydrate complex. Comparable FTIR assignments for oxygenated functional groups have been reported for graphene oxide-based nanocomposites [30].

Of particular relevance to rice straw, the silica-associated Si–O band at ~795 cm^{-1} exhibited a clear reduction in intensity following pretreatment, with transmittance increasing from approximately 65% to 75%. This spectroscopic observation independently corroborates the 34.4% reduction in silica content

quantified by ashing/selective dissolution (**Table 7**) and provides direct molecular evidence that the sono-Fenton process partially disrupts the Si–O–Si network in the rice straw epidermal silica layer. To the best of our knowledge, simultaneous spectroscopic confirmation of both lignin removal and silica disruption in a single-step sono-Fenton process has not been previously reported for rice straw.

SEM morphological analysis

SEM micrographs of rice straw before and after sono-Fenton pretreatment, both acquired at 3000x magnification with a 20 µm scale bar (**Figure 4**), reveal pronounced morphological disruption of the biomass following pretreatment, providing visual confirmation of the structural changes inferred from compositional and spectroscopic data.

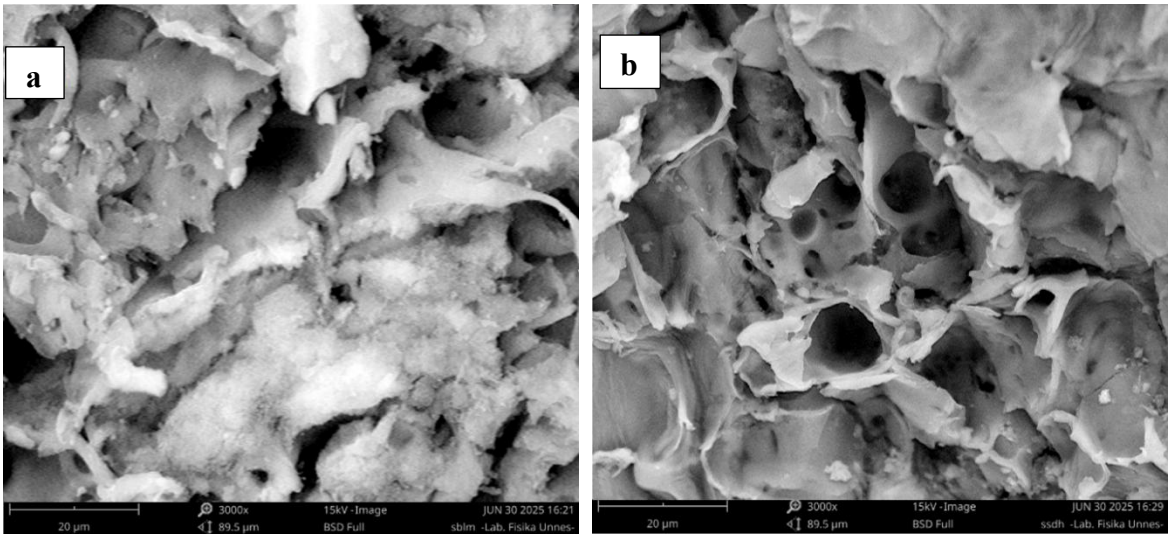


Figure 4 SEM micrographs of rice straw at 3000x magnification: (a) before sono-Fenton pretreatment, showing a compact, agglomerated surface with fused matrix material; (b) after sono-Fenton pretreatment under optimum conditions, showing extensive morphological disruption with exposure of underlying organized substructures.

The raw rice straw (**Figure 4(a)**) exhibits a compact, irregularly textured surface in which individual structural features are obscured by an overlying matrix of amorphous material. Small, rounded particulate features can be observed on the surface, consistent with mineral deposits—predominantly silica bodies and waxy cuticular components characteristic of the rice straw epidermis. The overall surface appears continuous and densely packed, with no clear evidence of internal porosity or accessible cellulose fibers, consistent with the well-documented recalcitrance of untreated rice straw to enzymatic attack [20].

In marked contrast, the pretreated rice straw (**Figure 4(b)**) exhibits extensive morphological disruption: The previously compact surface matrix appears fragmented and delaminated, exposing underlying fibrous substructures, while the rounded particulate silica deposits prominent in the raw sample are largely no longer evident on the visible surface, providing morphological corroboration of the 34.4% silica removal quantified by ashing (**Table 7**) and the reduction of the Si–O band observed in FTIR (**Figure 3**). Together, these morphological observations are consistent with a pretreatment mechanism in which oxidative attack by surface-generated •OH radicals on the catalyst, combined with mechanical effects from acoustic cavitation, disrupts the protective lignin-silica composite layer of the rice straw epidermis and exposes the underlying cellulose-rich substructure for subsequent enzymatic conversion. Scanning electron microscopy has likewise been employed to characterise the surface morphology of graphene oxide-based nanomaterials in related catalytic and environmental studies [31,32].

Comparison with other pretreatment methods for rice straw

To contextualize the performance of the present sono-Fenton system within the broader landscape of rice straw pretreatment technologies, **Table 8** compares delignification efficiency, silica removal, and operating conditions across representative methods reported in the literature. The data demonstrate that the present process achieves competitive delignification (78.4%) at moderate operating conditions (58 °C, 37 min, atmospheric pressure), without the use of corrosive chemicals or elevated pressures.

Table 8 Comparison of representative pretreatment methods for rice straw.

Method	Conditions	Delignification (%)	Silica removal (%)	Catalyst recovery	Ref.
Alkaline (NaOH)	2% NaOH, 121 °C, 60 min	65 - 75	~80*	No	[33]
Dilute acid	0.75% H_2SO_4 + boric acid, 150 °C, 20 min	~44	~48.5	No	[34]
Microwave + ultrasonic	Two-step microwave/US, alkaline	84.5	Not reported	No	[35]
Ultrasonic alone	450 kJ/kg TS, water medium	70.3	Not reported	N/A	[36]
US-assisted ionic liquid	[TEA][HSO_4], 130 °C, 30 min	74.9	Not reported	Partial (IL recycle)	[37]
Homogeneous Fenton	Fe^{2+}/H_2O_2, acidic medium (pH 2 - 4)	High lignin oxidation efficiency	Not reported	No (iron sludge generated)	[10,21]
Conventional Sono-Fenton	Ultrasound + dissolved Fe^{2+}/H_2O_2	Enhanced oxidation efficiency	Not reported	Limited (catalyst not readily separated)	[10,21]
Sono-Fenton (this work)	**2.7 wt% Fe_3O_4/GO, 58 °C, 37 min, 40 kHz**	**78.4**	**34.4**	**Yes (magnetic)**	**This work**

*Estimated from total ash reduction; specific silica quantification not reported.

Three observations from **Table 8** are noteworthy. First, while microwave-coupled ultrasonic methods can achieve marginally higher delignification (~84%) [35], and ultrasound alone or ultrasound-assisted ionic liquid can reach 70.3% and 74.9%, respectively [36,37], these routes require multi-step processing, elevated temperatures, or costly solvents, increasing both energy demand and process complexity. Second, conventional alkaline and dilute-acid methods [33,34] remove silica effectively but generate large volumes of corrosive waste and require neutralization before downstream enzymatic processing. Third, the present sono-Fenton system uniquely combines competitive delignification, quantified silica removal, and ready magnetic separability of the catalyst, a combination that, to the best of our knowledge, has not been simultaneously demonstrated in previous reports for rice straw. This comparison nonetheless reflects single-use performance, and the catalytic reusability of the present system relative to the recyclable ionic-liquid process listed in **Table 8** remains to be established.

Conclusions

A sono-Fenton heterogeneous system employing Fe_3O_4/GO nanocomposite as a magnetically recoverable catalyst was systematically optimized for rice straw delignification. CCD face-centered RSM identified temperature as the most influential factor, with optimum conditions (2.7 wt%, 58 °C, 37 min) achieving 78.4% delignification (prediction error 1.5%). The synergistic effect of ultrasound and catalyst exceeded the sum of individual treatments by 15.4 percentage points, with the synergy attributed predominantly to a radical-mediated mechanism enhanced by improved mass

transfer and continuous regeneration of catalytically active surface sites. Pseudo-first-order kinetics with E_a = 31.5 kJ/mol, $\Delta H^{\ddagger}$ = 28.8 kJ/mol, and $\Delta S^{\ddagger}$ = −222 $J \cdot mol^{-1} \cdot K^{-1}$ confirmed a chemically controlled, associative mechanism. FTIR spectra confirmed selective removal of lignin (markedly attenuated peaks at 1,730, 1,600, and 1,505 cm^{-1}) and partial disruption of the silica layer (reduced Si–O band at 795 cm^{-1}), while SEM micrographs revealed pronounced morphological disruption with exposure of underlying organized substructures. HPLC analysis revealed that inhibitor concentrations in the filtrate remained below critical thresholds, ensuring compatibility with downstream enzymatic hydrolysis. The sono-Fenton process uniquely reduced silica content by 34.4% while enriching cellulose to 52.8%. We acknowledge that the actual acoustic power delivered to the reaction medium was not calibrated by calorimetric methods; reported power values represent nominal electrical input. Future work should incorporate calorimetric calibration to enable energy-normalized comparison with other sonochemical pretreatment systems and to facilitate scale-up considerations. Although the Fe_3O_4/GO nanocatalyst demonstrated effective magnetic recoverability, catalyst reusability and iron leaching were not investigated in the present work. Future work should include catalyst reuse cycles, iron-leaching assessment, acoustic-power calibration, and long-term operational stability evaluation under repeated sono-Fenton conditions. Such studies will be essential to establish the techno-economic feasibility and industrial applicability of this pretreatment technology. Nevertheless, the comprehensive kinetic, thermodynamic, spectroscopic, and morphological evidence presented herein provides a rational design framework for sono-Fenton pretreatment of rice straw in lignocellulosic biorefinery applications.

Acknowledgements

The authors would like to express their sincere gratitude to the Biomass Processing Technology Laboratory, Faculty of Engineering, Universitas Negeri Semarang, Semarang 50299, Indonesia for providing the research facilities and technical support necessary for conducting this study.

Declaration of Generative AI in Scientific Writing

The authors recognize that generative AI tools (such as QuillBot and OpenAI's ChatGPT) were utilized during the preparation of this manuscript, solely to assist with language refinement and grammar editing. No sections of the content were generated, nor was any data interpreted, by AI. The authors assume complete responsibility for the work's content and the conclusions drawn

CRediT author statement

Hanif Ardhiansyah: Conceptualization, Data curation, Formal analysis, Investigation, Methodology, Writing – original draft, writing – review & editing. **Tutuk Djoko Kusworo**: Supervise methodology, conceptualization, data curation, formal analysis, and writing – review & editing. **Andri Cahyo Kumoro**: Supervise, methodology, conceptualization, data curation, formal analysis, writing – review & editing.

References

[1] Food and Agriculture Organization of the United Nations. *World food and agriculture - Statistical yearbook 2020*. FAO, Rome, Italy, 2020.

[2] T Lepage, M Kammoun, Q Schmetz and A Richel. Biomass-to-hydrogen: A review of main routes production, processes evaluation and techno-economical assessment. *Biomass Bioenergy* 2021; **144**, 105920.

[3] Q Huang, YP Tang, ZF Zhang, Z Wang and L Dai. Catalytic asymmetric transformation of platform chemicals derived from lignocellulosic biomass. *Chemical Communications* 2025; **61(50)**, 8960-8968.

[4] TK Tran, CK Trinh, GH Tran, TL Luong, AT Nguyen, HJ Leu, VD Le and N Kim. The utilization of rice straw (*Oryza Sativa L.*) as a green catalyst in the enhanced production of hydrogen via the thermochemical conversion process of shrimp farm sludge. *International Journal of Hydrogen Energy* 2024; **52**, 32-45.

[5] J Sun, R Ding and J Yin. Pretreatment corn ingredient biomass with high pressure CO_2 for conversion to fermentable sugars via enzymatic hydrolysis of cellulose. *Industrial Crops and Products* 2022; **177**, 114518.

[6] G Sharma, M Kumar, AK Pandey, S Kumari, A Singh, NA Ansari and NA Gaur. Pretreatment technologies for valorisation of lignocellulosic biomass towards sustainable biorefineries: Comprehensive insights and advances. *Bioresource Technology Reports* 2025; **32**, 102336.

[7] H Ardhiansyah, M Kusumaningrum, ZAS Bahlawan, H Prasetiawan, F Savanti and HA Fauziyyah. Green pretreatment techniques for enhanced delignification of lignocellulosic biomass: A case study of biomass waste in Indonesia. *IOP Conference Series: Earth and Environmental Science* 2024; **1381**, 012034.

[8] A Kheto, A Chaudhari, S Manikpuri, R Sehrawat, K Gul, L Kumar and KA Khan. Effect of ultrasonic-pretreatment on soaking kinetics, nutritional, anti-nutritional, and functional properties of guar seeds. *LWT* 2024; **213**, 117046.

[9] Z Qin, L Cheng, L Liu, R Zhang, S Zhao and L Ma. Combined effects of organic solvent and ultrasonic pretreatments on cellulose fiber extraction from hemp. *Industrial Crops and Products* 2024; **220**, 119436.

[10] AY Ghjeer and AH Abbar. A comparative study of four technologies (Fenton, Sono-Fenton (SF), Electro-Fenton (EF), and Sono-Electro-Fenton (SEF)) for hospital wastewater treatment. *Case Studies in Chemical and Environmental Engineering* 2023; **8**, 100519.

[11] RF Abbas, MJM Hassan and AM Rheima. Adsorption of fast green dye onto Fe_3O_4 MNPs and GO/Fe_3O_4 MNPs synthesized by photo-irradiation method: Isotherms, thermodynamics, kinetics, and reuse studies. *Sustainable Chemistry for the Environment* 2024; **6**, 100104.

[12] M Moghaddam-Manesh, R Darvishi, A Barati, A Moshkriz and M Seyedsharifi. Synthesis of novel Fe_3O_4@gly@Indole@$CuNO_3$ magnetic nanoparticle as high-performance antibiotic absorbent, antimicrobial agent, and reusable magnetic Nano catalyst. *Journal of Environmental Chemical Engineering* 2025; **13(1)**, 114970.

[13] SIA Shah, W Ahmad, M Anwar, R Shah, JA Khan, NS Shah, A Al-Anazi and C Han. Synthesis, properties, and applications of Fe_3O_4 and Fe_3O_4-based nanocomposites: A review. *Applied Catalysis O: Open* 2025; **203**, 207049.

[14] C Donga, SB Mishra, LN Ndlovu, AS Abd-El-Aziz, AT Kuvarega and AK Mishra. Magnetic magnetite-graphene oxide (Fe_3O_4-GO) nanocomposites for removal of dyes from aqueous solution. *Journal of Inorganic and Organometallic Polymers and Materials* 2024; **34**, 4192-4202.

[15] J Waluyo, FC Abimanyu, FY Widharmo, SH Pranolo, M Kaavessina, I Kurnia and IT Purba. Co-precipitated magnetic graphene oxide nanocomposites for methyl orange uptake: Isotherm, kinetic, and regeneration. *Results in Chemistry* 2025; **18**, 102790.

[16] H Ardhiansyah, TD Kusworo and AC Kumoro. Enhanced structural stability of Fe_3O_4/GO–PEG nanocomposite for ultrasonic pretreatment applications. *Trends in Sciences* 2026; **23(6)**, 12444.

[17] PJV Soest, JB Robertson and BA Lewis. Methods for dietary fiber, neutral detergent fiber, and nonstarch polysaccharides in relation to animal nutrition. *Journal of Dairy Science* 1991; **74(10)**, 3583-3597.

[18] Technical Association of the Pulp and Paper Industry. *Acid-insoluble ash in wood and pulp (TAPPI T 244 cm-99)*. TAPPI, Karnataka, India, 1999.

[19]L Segal, JJ Creely, AE Martin Jr and CM Conrad. An empirical method for estimating the degree of crystallinity of native cellulose using the x-ray diffractometer. *Textile Research Journal* 1959; **29(10)**, 786-794.

[20] MC Maguyon-Detras, MVP Migo, NV Hung and M Gummert. *Thermochemical Conversion of Rice Straw.* Springer, Switzerland, 2019, p. 43-64.

[21] M Munoz, ZM de Pedro, JA Casas and JJ Rodriguez. Preparation of magnetite-based catalysts and their application in heterogeneous Fenton oxidation - A review. *Applied Catalysis B: Environmental* 2015; **176-177**, 249-265.

[22] S Merouani, A Dehane, O Hamdaoui and M Ashokkumar. Review of ultrasonication-assisted Fenton processes for degrading aqueous pollutants. *Ultrasonics Sonochemistry* 2026; **124**, 107725.

[23]Y Kawamata, T Yoshikawa, H Aoki, Y Koyama, Y Nakasaka, M Yoshida and T Masuda. Kinetic analysis of delignification of cedar wood during organosolv treatment with a two-phase solvent using the unreacted-core model. *Chemical Engineering Journal* 2019; **368**, 71-78.

[24] S Sarma, VK Dubey and VS Moholkar. Kinetic and thermodynamic analysis (with statistical optimization) of hydrogen production from crude glycerol using *Clostridium pasteurianum*. *International Journal of Hydrogen Energy* 2016; **41(44)**, 19972-19989.

[25] MJ Taherzadeh and K Karimi. Enzyme-based hydrolysis processes for ethanol from lignocellulosic materials: A Review. *BioResources* 2007; **2(4)**, 707-738.

[26] E Palmqvist and B Hahn-Hägerdal. Fermentation of lignocellulosic hydrolysates. II: Inhibitors and mechanisms of inhibition. *Bioresource Technology* 2000; **74(1)**, 25-33.

[27] LJ Jönsson and C Martín. Pretreatment of lignocellulose: Formation of inhibitory by-products and strategies for minimizing their effects. *Bioresource Technology* 2016; **199**, 103-112.

[28] EJ Yazdi, GJW Euverink and J Yue. Pretreatment and enzymatic hydrolysis of tertiary cellulose for glucose production. *Industrial Crops and Products* 2025; **237**, 122144.

[29] M Schwanninger, JC Rodrigues, H Pereira and B Hinterstoisser. Effects of short-time vibratory ball milling on the shape of FT-IR spectra of wood and cellulose. *Vibrational Spectroscopy* 2004; **36(1)**, 23-40.

[30] P Basnet, PK Jha, A Gupta and S Chatterjee. Synergistic effect of Tea-phytochemicals, Noble metals and Zno Nano-Photo-Composites for combating resistance of bacterial growth. *Journal of Nano Research* 2021; **70**, 53-66.

[31] PK Jha, W Khongnakorn, C Chawenjkigwanich, MS Chowdhury and K Techato. Eco-friendly reduced graphene oxide nanofilter preparation and application for iron removal. *Separations* 2021; **8(5)**, 68.

[32] PK Jha, C Chawengkijwanich, K Techato, W Limbut and M Luengchavanon. Callistemon viminalis leaf extract mediated biosynthesis of Ag, rGO-Ag-ZnO nanomaterials for catalytic PEM fuel cell application. *Trends in Sciences* 2022; **19(11)**, 493.

[33] SS Singh, LT Lim and A Manickavasagan. Ultrasound-assisted alkali-urea pre-treatment of *Miscanthus* × giganteus for enhanced extraction of cellulose fiber. *Carbohydrate Polymers* 2020; **247**, 116758.

[34] T Chiranjeevi, AJ Mattam, KK Vishwakarma, A Uma, VCR Peddy, S Gandham and HR Velankar. Assisted single-step acid pretreatment process for enhanced delignification of rice straw for bioethanol production. *ACS Sustainable Chemistry & Engineering* 2018; **6(7)**, 8762-8774.

[35] ACF Louis, S Venkatachalam and S Gupta. Innovative strategy for rice straw valorization into nanocellulose and nanohemicellulose and its application. *Industrial Crops and Products* 2022; **179**, 114695.

[36] YK Ravi, S Kavitha, S Palani, G Kumar and RJ Banu. Ultrasonic induced mechanoacoustic effect on delignification of rice straw for cost effective biopretreatment and biomethane recovery. *Sustainable Energy & Fuels* 2021; **5(6)**, 1832-1844.

[37] Z Ziaei-Rad, M Pazouki, J Fooladi, M Azin, SN Gummadi and A Allahverdi. Investigation of a robust pretreatment technique based on ultrasound-assisted, cost-effective ionic liquid for enhancing saccharification and bioethanol production from wheat straw. *Scientific Reports* 2023; **13**, 446.